

Influence of Silicate Concentration in Electrolyte on the Growth and Performance of Plasma Electrolytic Oxidation Coatings Prepared on Low Carbon Steel

Wenbin Yang, Zhenjun Peng, Baixing Liu, Weimin Liu, and Jun Liang

(Submitted January 18, 2017; in revised form November 12, 2017; published online April 12, 2018)

Plasma electrolytic oxidation (PEO) coatings were prepared on low carbon steel from electrolytes with different silicate concentrations. The microstructure, elemental and phase compositions of the PEO coatings were analyzed by scanning electron microscope, energy-dispersive spectrometer, and x-ray diffraction, respectively. The adhesion of PEO coatings with low carbon steel substrate was qualitatively examined by thermal shock tests. The tribological properties were evaluated by a reciprocating tribometer sliding against a Si_3N_4 ceramic ball. The corrosion behaviors of PEO coatings were investigated in 3.5 wt.% NaCl solution by electrochemical impedance spectra and potentiodynamic polarization. Results indicated that all the PEO coatings were comprised of amorphous SiO_2 and Fe-containing oxides; however, the silicate concentration in electrolyte showed significant influence on the growth and the performance of PEO coatings. The PEO coating prepared from the electrolyte with silicate concentration of 30 g/L had the highest Fe content because the substrate was more readily oxidized and showed a dense structure, resulting in the best comprehensive performance of adhesion, wear resistance, and corrosion resistance.

Keywords adhesion, corrosion, growth process, plasma electrolytic oxidation, silicate concentration, tribological property

1. Introduction

Low carbon steel has been widely used in variety of industries, due to its advantages, such as good processability, high strength, and low cost (Ref 1), while the poor wear and corrosion resistance should be highly regarded, because these drawbacks usually cause failures of carbon steel structures or parts. To improve the wear or corrosion resistance of low carbon steel, surface technologies are used to modify carbon steel surface, such as electroplating (Ref 2), thermal spraying (Ref 3), P/CVD (Ref 4, 5), and so on. Plasma electrolytic oxidation (PEO) developed as an environmentally friendly technique can be used to prepare ceramic coatings on metal surface from electrolyte with specific composition (Ref 6). The ceramic coating characterized by micropores and microcracks shows a porous structure and excellent comprehensive performance of high corrosion resistance and wear resistance (Ref 7, 8). Moreover, the composition of PEO coatings can be controlled conveniently by adjusting the composition of the electrolytes (Ref 9).

So far, most researches about PEO have been focused on valve metals (Al, Mg, Ti, or their alloys) (Ref 10-12). However,

the application of PEO technology on carbon steel has been just attempted. It was found that PEO coatings could be successfully prepared on carbon steel from a few electrolytes, such as carbonate electrolyte, aluminate electrolyte, and silicate electrolyte (Ref 13-15). The PEO coatings prepared from these electrolytes showed a similar porous structure and improved the wear or corrosion resistance of carbon steel substrate. It was also reported that the composite coatings containing hydrophobic, superhydrophobic, or organic layers in combination with PEO coating can be prepared on low carbon steel and the PEO sublayer played an important role in improving the corrosion resistance of the composite coatings (Ref 16, 17). However, up to now, the researches mainly focused on the preparation, structural characterization, and performance of PEO coatings from aluminate and silicate electrolytes. However, the growth process of PEO coatings can be influenced by many parameters, such as current density, frequency, and composition of electrolyte, etc. Reportedly, the concentration of main component in electrolyte has a significant impact on the growth process and properties of PEO coatings (Ref 18).

In this work, PEO coatings were prepared on low carbon steel substrate from electrolytes with different silicate concentrations (10, 20, 30, 40, and 50 g/L). The influence of silicate concentrations in electrolytes on the growth and properties of PEO coatings was investigated.

2. Experimental

2.1 Preparation of PEO Coatings

Low carbon steel plates cut into 25 mm × 20 mm × 8 mm were used in this work. The nominal weight percentage of elements in the substrate was 0.14-0.22 C%, 0.30-0.65 Mn%, ≤ 0.30 Si%, ≤ 0.045 P%, ≤ 0.05 S%, and Fe

Wenbin Yang, State Key Laboratory of Solid Lubrication, Lanzhou Institute of Chemical Physics, Chinese Academy of Sciences, Lanzhou 730000, China; and University of Chinese Academy of Sciences, Beijing 100039, China; **Zhenjun Peng**, **Baixing Liu**, **Weimin Liu**, and **Jun Liang**, State Key Laboratory of Solid Lubrication, Lanzhou Institute of Chemical Physics, Chinese Academy of Sciences, Lanzhou 730000, China. Contact e-mail: jliang@licp.cas.cn.

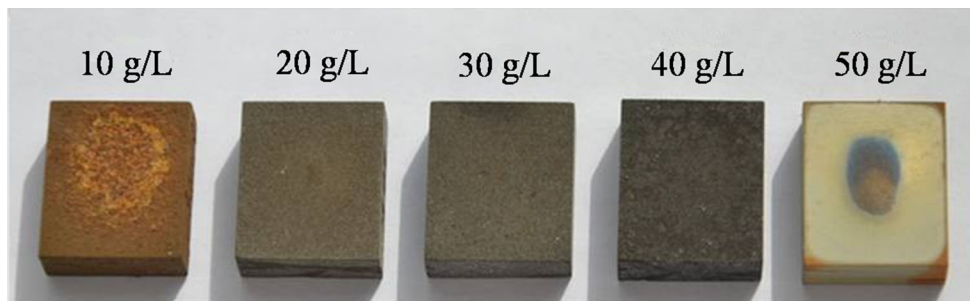


Fig. 1 Optical images of PEO coatings corresponding to electrolytes with different silicate concentrations

balance. Before the PEO process, low carbon steel plates have been polished by 1000#, 1500#, and 2000# abrasive papers orderly with water lubrication, ultrasonically decontaminated by deionized water and degreased by acetone, and then dried by air. The PEO process was performed by a system composing of a pulsed bipolar power supply, a stainless container, an electromagnetic stirring system, and a cooling system. The low carbon steel plate and the spiral stainless cooling pipe were used as the anode and cathode, respectively. The PEO process was performed in electrolytes with various silicate concentrations. The concentration of $\text{NaH}_2\text{PO}_4 \cdot \text{H}_2\text{O}$ in all electrolytes was 1.2 g/L, and the concentrations of $\text{Na}_2\text{SiO}_3 \cdot 9\text{H}_2\text{O}$ in the electrolytes marked S1, S2, S3, S4, and S5 were (in g/L) 10, 20, 30, 40, and 50, respectively. The PEO coatings related to the electrolytes were abbreviated as S1 coating, S2 coating, S3 coating, S4 coating, and S5 coating. The higher duty cycle is bad for the increase of the potential under constant current mode. Therefore, the current density during PEO process was kept at 0.12 A/cm^2 . The frequency was 150 Hz and the duty cycle was 3%. To eliminate the influence of thickness on properties of PEO coatings, samples were treated for different time from different electrolytes to obtain PEO coatings of similar thickness.

2.2 Characterization of Structures and Compositions

The optical images of PEO coatings prepared from electrolytes with different silicate concentrations were recorded by a digital camera. The surface, cross section, and wear tracks were observed by scanning electron microscope (SEM, JSM-5600LV) under the secondary electron mode. The elemental composition was investigated by the energy-dispersive spectrometer (EDS). The phase composition was analyzed by x-ray diffraction (XRD, Rigaku D/Max-2400 x-ray diffractometer).

2.3 Mechanical Tests

The adhesion of PEO coatings was examined by thermal shock test. Firstly, the furnace was heated up to $500 \text{ }^\circ\text{C}$; secondly, the samples were kept in the furnace for at least 10 min making sure the samples were heated thoroughly; lastly, the samples were taken out of the furnace quickly and immersed in a basin of cool tap water with a temperature of about $20 \text{ }^\circ\text{C}$. The cycles were repeated until failures of the PEO coating appeared. The failures are indicated by the occurrence of localized flaking off of PEO coatings. The PEO coating with good adhesion is characterized by more thermal shock cycles before local falling off happens.

2.4 Tribological Tests

The tribological properties of PEO coatings prepared in S2, S3, and S4 were evaluated by a UMT Tribolab tester. A Si_3N_4 ceramic ball with the diameter of 6.35 mm was used as the counterpart sliding against PEO coatings. The dry sliding was performed with the load of 5 N at the linear speed of 0.1 m/s. The wear rates were measured by a 3D profilometer (USA, NanoMap500LS).

2.5 Corrosion Tests

The electrochemical tests on low carbon steel substrate and PEO coatings prepared from electrolytes with various silicate concentrations were performed using an AUTOLAB PGSTAT 302N. A three-electrode system (a platinum sheet as the counter electrode, an Ag/AgCl electrode as the reference electrode, and the sample as the working electrode) was applied during the tests. The potentiodynamic polarization curves and electrochemical impedance spectroscopy (EIS) were measured to investigate the corrosion behavior of samples in 3.5 wt.% NaCl solution. The potentiodynamic polarization was performed at a scan rate of 1 mV/s. The EIS was carried out at the open circuit potential with an AC amplitude of 10 mV over the frequency of $0.01\text{-}10^5 \text{ Hz}$.

The immersion test was introduced to further investigate the corrosion behavior of different PEO coatings. The samples covered by PEO coatings were immersed in 3.5 wt.% NaCl solution at room temperature for 120 h. After the immersion test, the morphologies of different PEO coatings were observed by SEM.

3. Results and Discussion

3.1 The Behavior of Time–Voltage Curves

Figure 1 shows the optical images of samples prepared by PEO from electrolytes with different silicate concentrations. It can be seen that uniform PEO coatings could be successfully prepared from electrolytes with silicate concentrations of 20, 30, and 40 g/L. Therefore, only the electrolytes with silicate concentrations of 20, 30, and 40 g/L were discussed in the following context. The positive voltage evolution curves during PEO process of low carbon steel in electrolytes with different silicate concentrations are shown in Fig. 2. It can be found from Fig. 2 that three main stages can be identified for all three curves. In the first stage (stage I), the voltage sharply increased due to the formation of gas envelope (with the main compo-

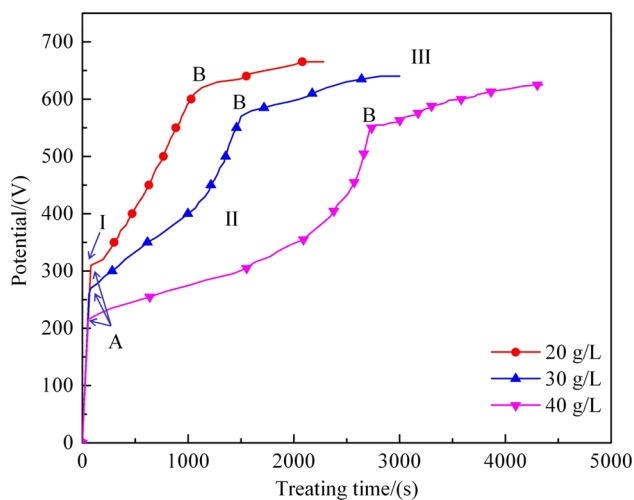


Fig. 2 Curves of voltage vs. treating time during PEO process in electrolytes with different silicate concentrations

sition of oxygen) around the sample and the generation of initial dielectric coating on the substrate (Ref 19). In stage I, no apparent sparks could be observed on the substrate surface. With the voltage increasing, an inflection point corresponding to the breakdown voltage (point A) occurred. At the breakdown voltage, fine sparks appeared on the surface of the sample. The breakdown voltage for each curves decreased with the increase in silicate concentration, due to the increase in electrical conductivity of electrolytes (18.0, 25.2, and 31.7 mS/cm corresponding to electrolytes with silicate concentrations of 20, 30, and 40 g/L) (Ref 20). During the second stage (stage II), fine sparks distributed firstly around the edge of the sample to form a local rust-colored film and then gradually expanded to the center of the sample. Subsequently, the whole sample was covered by fine sparks and a uniform rust-colored film was formed. Another inflection point corresponds to the critical voltage (point B) for the uniform distribution of sparks on substrate surface. Beyond the critical voltage (stage III), the size of sparks increased and the number decreased over time. The voltage during stage III increased slowly and evenly due to the uniform growth of PEO coating caused by the uniform sparks. However, the critical voltage related to each electrolyte decreased with the increase in silicate concentration, i.e., the increase in electrical conductivity (Ref 21). A higher electrical conductivity led to applying higher voltage to break down the resistance of the dielectric layer, resulting in a lower breakdown voltage. Reasonably, the higher electrical conductivity can lead to a lower critical voltage for the uniform distribution of sparks. To obtain similar coating thickness, the duration of PEO treatment, especially the duration of stage III, was prolonged with increasing silicate concentration in electrolyte, due to an inversely proportional relationship between growth rate and electrical conductivity (Ref 22).

3.2 Surface Morphologies and Compositions

The surface morphologies of PEO coatings prepared from electrolytes with different silicate concentrations are presented in Fig. 3. All of the coatings were featured by typical characteristics of PEO coatings comprising of micropores. The pores were created by the expulsion of melt products from micro-discharge channels to electrolyte and the subsequent

solidification (Ref 23). In the case of S2 coating (Fig. 3a), the micropores distributed unevenly and the number of the micropores was smaller in comparison with that of the micropores on the surface of S3 and S4 coatings, suggesting that the discharge on the surface of S2 coating was rougher. Additionally, the surface of S2 coating was covered by lots of porous oxide particles (Fig. 3c), while the surface of S3 coating was characterized by an increasing number and uniform distribution of micropores. Besides, S3 coating was much denser with less porous oxide particles. For S4 coating, the number of micropores on the surface was much larger than that of S2 and S3 coatings. Besides, there were many small micropores on the surface and around the oxide particles.

The results of EDS analysis of PEO coatings prepared from electrolytes with different silicate concentrations are listed in Table 1. It can be seen that all three PEO coatings were comprised of elements Fe, Si, and O, indicating that the element compositions of PEO coatings were mainly from the substrate and electrolyte. However, the constituents of the coatings significantly depended on the composition of electrolyte. It can be seen that the S3 coating had the highest Fe content (47.56 wt.%) while the S4 coating had the highest Si content (44.93 wt.%). The highest Fe content for the S3 coating suggested that the substrate was more prone to be oxidized during the PEO process occurring in electrolyte with silicate concentration of 30 g/L.

The XRD patterns presented in Fig. 4 clearly show that the characteristic diffraction peaks of Fe_2O_3 and Fe_3O_4 can be identified for all the PEO coatings. Additionally, a broad and weak diffraction peak located in the 2θ range of $20^\circ \sim 25^\circ$ in the XRD patterns belongs to amorphous SiO_2 (Ref 24), suggesting that amorphous SiO_2 is produced in the three electrolytes with different silicate concentrations during the PEO process. Conclusively, the PEO coatings prepared from the electrolytes with different silicate concentrations possess nearly the same phase compositions.

3.3 Cross-Sectional Morphologies

Figure 5(a), (b), and (c) shows the cross-sectional morphologies of PEO coatings on low carbon steel prepared from electrolytes with different silicate concentrations. It can be found from Fig. 5 that all the PEO coatings grew inward and outward relative to the original surface of the substrate, suggesting that the substrate participated in the formation of PEO coatings (Ref 25). Apparently, in the case of S2 coating, the PEO coating grew toward substrate for about $15 \mu\text{m}$ (Fig. 5a). There were many micropores or cracks inside S2 coating and at the interface between S2 coating and substrate, leading to a more porous structure. The micropores and cracks at the interface would probably have negative influence on the adhesion of the coating with substrate. For S3 coating (Fig. 5b), the PEO coating grew inward for more than $20 \mu\text{m}$ and fewer micropores or cracks could be found inside the coating or at the interface. The observation result suggested that more substrate was oxidized to form PEO coating during the PEO process in electrolyte with silicate concentration of 30 g/L. Moreover, it also indicated that S3 coating had much more dense structure and probably good adhesion with substrate. But for S4 coating, the maximum depth that PEO coating grew inward was only about $8 \mu\text{m}$ (Fig. 5c), indicating that it was relatively difficult for substrate to be oxidized in electrolyte with silicate concentration of 40 g/L. Besides, many micropores could be

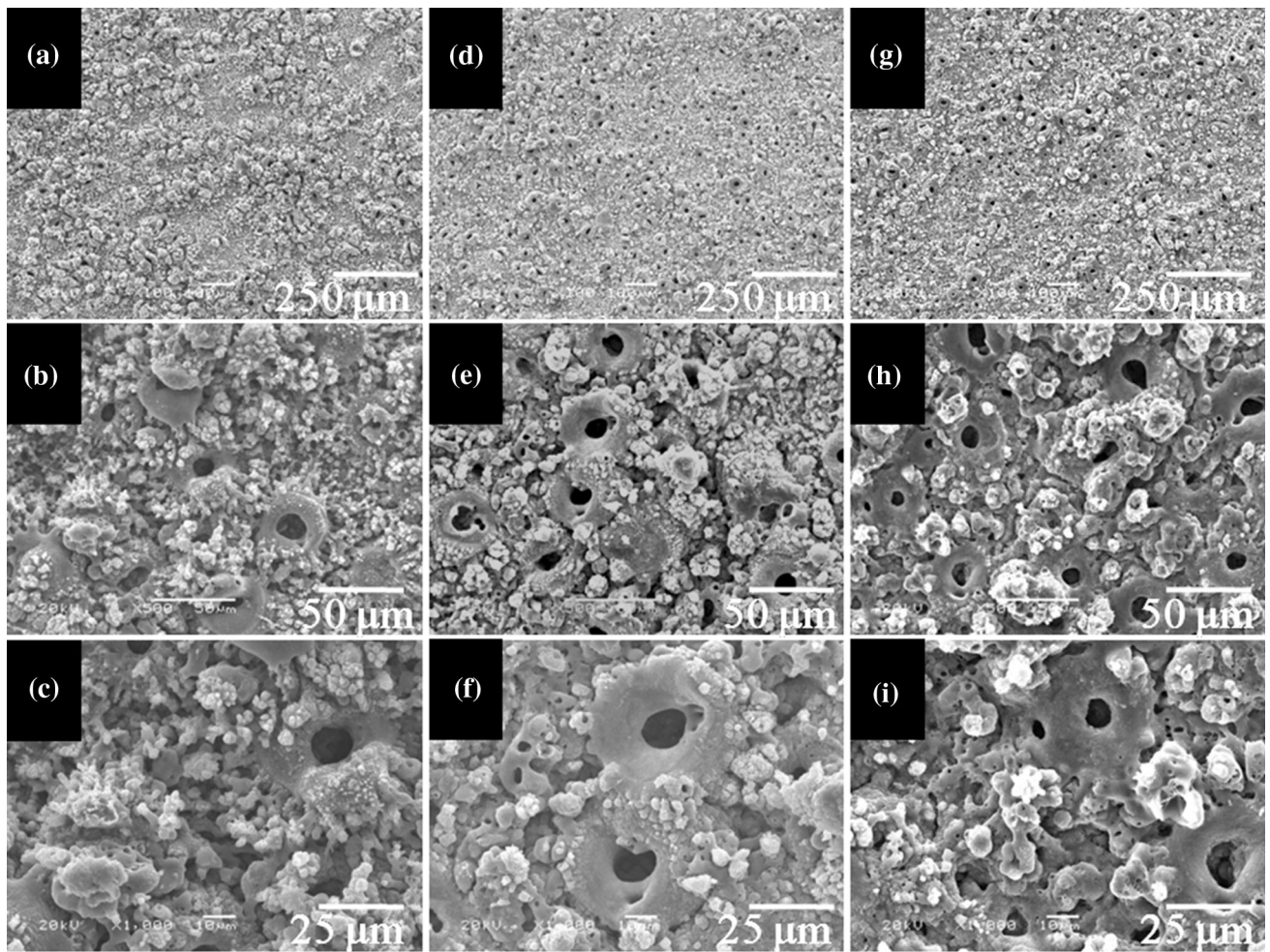


Fig. 3 Morphologies of PEO coatings prepared in electrolytes with different silicate concentrations: (a, b, c) S2 coating, (d, e, f) S3 coating, (g, h, i), S4 coating

Table 1 Main element compositions of PEO coatings prepared from electrolytes S2, S3, and S4, respectively

PEO coatings	Fe, wt. %	Si, wt. %	O, wt. %
S2 coating	37.23	29.16	31.49
S3 coating	47.56	22.82	25.26
S4 coating	21.94	44.93	41.13

observed inside the PEO coating but fewer at the interface between coating and substrate, suggesting a porous structure of S4 coating. In conclusion, the silicate concentration in electrolyte significantly influenced the growth of the PEO coatings. It was much easier for substrate to be oxidized in electrolyte with silicate concentration of 30 g/L, resulting in the highest content of Fe in S3 coating, shown in Table 1. Moreover, electrolyte with silicate concentration of 30 g/L is helpful to obtain PEO coating with a denser structure (Fig. 5b).

3.4 Thermal Shock Resistance of PEO Coatings

The thermal shock tests were conducted to investigate the influence of silicate concentration on thermal shock resistance (closely related to the adhesion) of PEO coatings with substrate, and the results are shown in Fig. 6. It can be seen that the edge

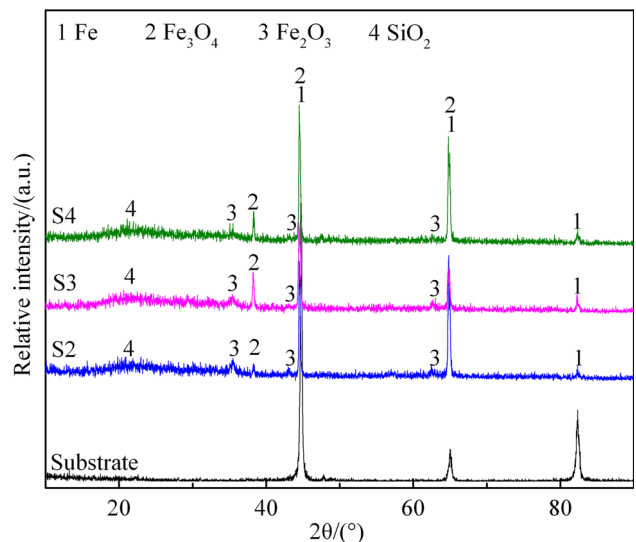


Fig. 4 XRD patterns of S2, S3, and S4 coatings

and the center of S2 coating began to peel off after eight shock cycles. However, the S3 and S4 coatings still kept intact. Only a slight peeling off at the center could be observed on S3 coating,

while S4 coating showed a complete failure after 20 shock cycles. The results of thermal shock tests suggest that the PEO coating prepared in electrolyte with silicate concentration of 30 g/L had the best shock resistance, which was consistent with the observations in Fig. 5 that the oxidation of substrate was beneficial to enhance the density and adhesion of PEO coating (Ref 26). Besides, the PEO coating at the center of samples was vulnerable to peeling off after thermal shock tests, due to the delay of spark discharges at the center of the sample compared with that on the edge of the sample (Ref 15).

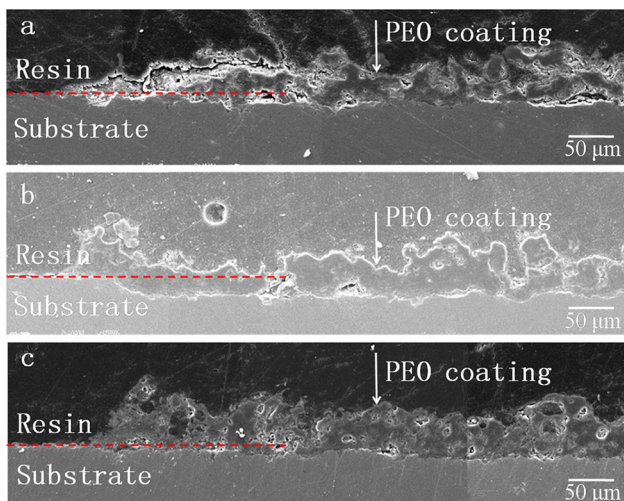


Fig. 5 Cross-sectional morphologies of PEO coatings prepared from different electrolytes: (a) S2 coating, (b) S3 coating, and (c) S4 coating

3.5 Tribological Properties

The friction coefficients versus sliding time for PEO coatings prepared in electrolytes with different silicate concentrations are shown in Fig. 7(a). It can be seen that all three PEO coatings exhibited friction coefficient $0.7 \sim 0.75$, indicating that silicate concentrations showed no influence on the friction behavior. It was because the silicate concentration in electrolyte did not fundamentally change the element (Table 1) and phase compositions of PEO coatings (Fig. 4).

The depth profiles of wear tracks of PEO coatings prepared in electrolytes with different silicate concentrations are shown in Fig. 7(b). The width and depth of wear track on S2 coating are found to be 1200 and 41 μm . S3 coating registers the width of about 800 μm and the depth of 32 μm in the wear track. It also can be found that the width and depth of wear track of S4 coating are about 880 and 37 μm . Besides, the wear rates of PEO coatings prepared in electrolytes with silicate concentrations of 20, 30, and 40 g/L were calculated to be $4.78 \times 10^{-4} \text{ mm}^3/(\text{N m})$, $3.12 \times 10^{-4} \text{ mm}^3/(\text{N m})$, and $3.52 \times 10^{-4} \text{ mm}^3/(\text{N m})$, respectively, shown in Fig. 7(c). It is obvious that the PEO coating prepared in electrolyte with silicate concentration of 30 g/L showed the best wear resistance, due to its denser structure and good adhesion with substrate.

The tribological properties of PEO coatings were further studied by comparing the SEM morphologies of wear tracks shown in Fig. 8. It can be seen that the worn surface of S2 coating was characterized by many wide scratch marks parallel to the sliding direction, resulted from abrasive wear. In addition, the severe detachment of S2 coating appeared on the worn surface, which resulted in deep craters filled with a large amount of debris. The detachment was due to the brittle fracture by normal stress cycling during sliding test. The presence of the debris enhanced the abrasive of PEO coating.

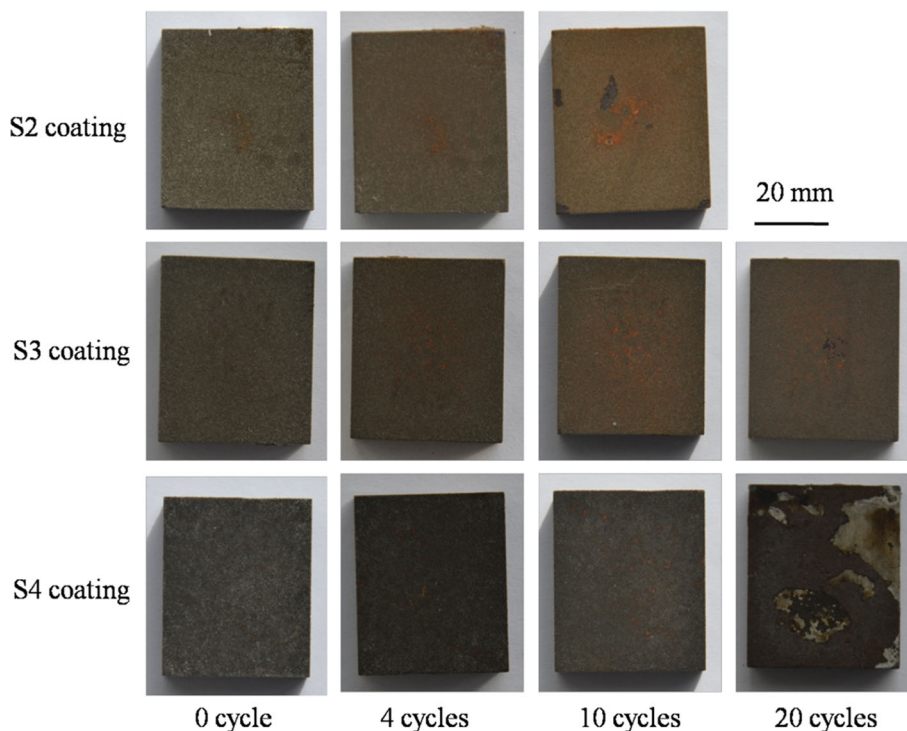


Fig. 6 Results of thermal shock tests for S2, S3, and S4 coatings

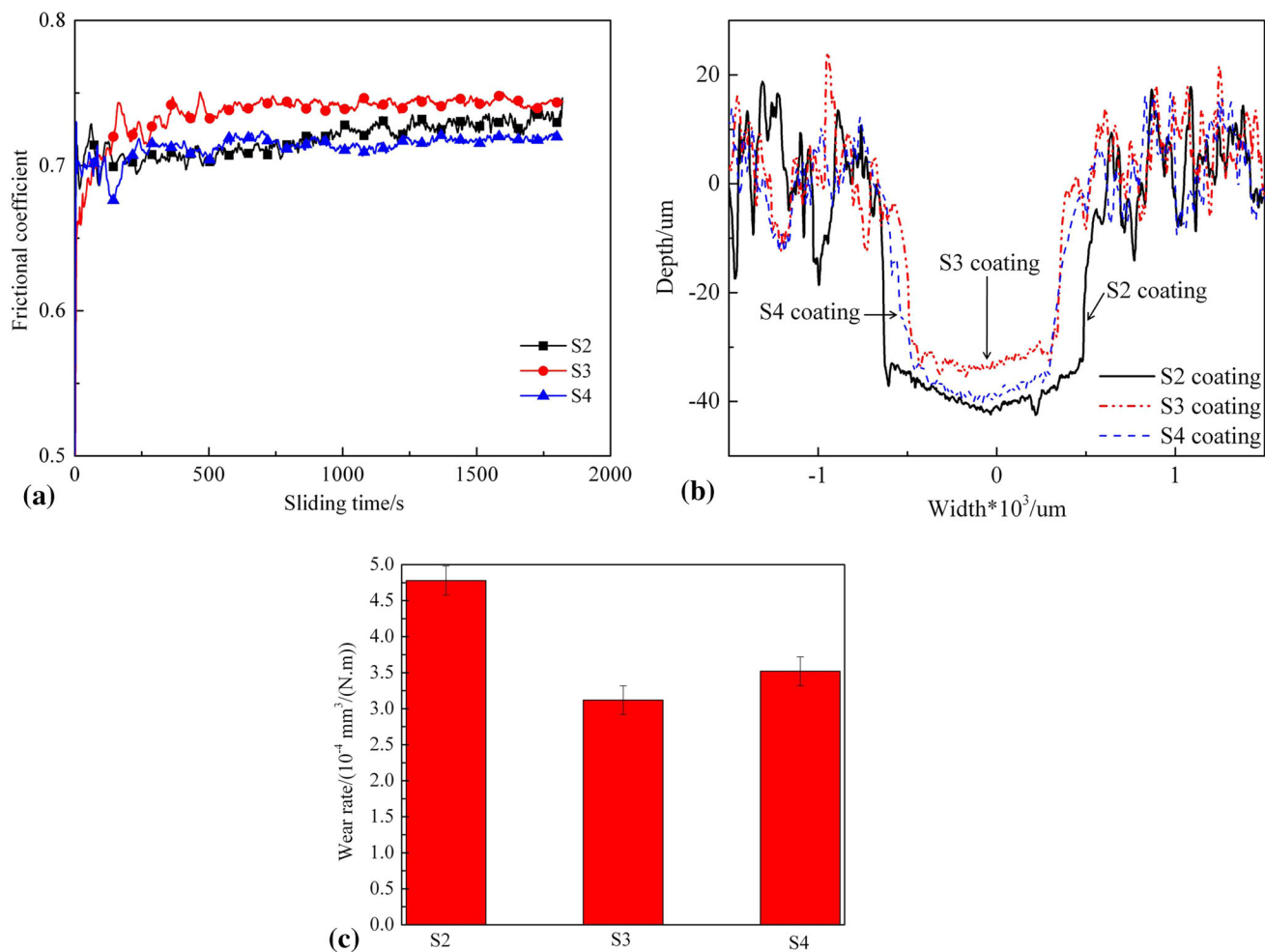


Fig. 7 (a) friction coefficients, (b) depth profiles of wear tracks, and (c) wear rates of S2, S3, and S4 coatings, respectively

Therefore, S2 coating showed the highest wear rate. For the S3 coating, the scratch marks and detachment were not so obvious on the worn surface ascribed to the dense structure and best adhesion with substrate. In the case of S4 coating, the width of scratch marks due to abrasive wear was also smaller, while the strips of detachment along sliding direction appeared, mainly resulted from shear stress cycling during sliding test.

3.6 Corrosion Behaviors

The potentiodynamic polarization curves of low carbon steel substrate and PEO coatings prepared from electrolytes with different silicate concentrations in 3.5 wt.% NaCl solution are depicted in Fig. 9. Generally, a coating with good corrosion resistance is characterized by more positive corrosion potential and lower corrosion current density (Ref 27, 28). It can be seen from Fig. 9 that all the PEO coatings prepared in electrolytes with different silicate concentrations show more positive corrosion potential and lower corrosion current density than the low carbon steel substrate, suggesting that the PEO coatings can offer a protection for carbon steel substrate to various degrees. The corrosion potential and corrosion current density of low carbon steel were -0.82 V and $5.25 \times 10^{-5} \text{ A/cm}^2$, respectively, while for S2, S3, and S4 coatings, the corrosion potentials and corrosion current densities were -0.54 V and $1.25 \times 10^{-5} \text{ A/cm}^2$, -0.35 V and $6.03 \times 10^{-6} \text{ A/cm}^2$, and -0.48 V and

$1.0 \times 10^{-5} \text{ A/cm}^2$, respectively. Obviously, the corrosion resistance of substrate coated by S3 coating could be most significantly improved by a shift of corrosion potential toward positive direction of 470 mV and a decrease of corrosion current density by about ten times of magnitude. The S4 coating exhibited a corrosion resistance with a positive shift of corrosion potential of 340 mV and a decrease of corrosion current density of about five times of magnitude, inferior to that of the S3 coating. The S2 coating showed the worst corrosion resistance among the three PEO coatings. The positive shift of corrosion potential and decrease of corrosion current density are only 280 mV and about four times of magnitude. The results of potentiodynamic polarization were in accordance with the cross-sectional morphologies shown in Fig. 5. The best corrosion resistance of the S3 coating was ascribed to the denser structure and better adhesion with substrate (Fig. 5b).

The Bode plots shown in Fig. 10 were used to further investigate the corrosion resistance of PEO coatings prepared from electrolytes with different silicate concentrations. The corrosion resistance of coatings can be represented by the impedance module in low-frequency region (Ref 29). It can be found from Fig. 10 that the low frequency impedance of substrate, S2, S3, and S4 coatings was about $1.3 \times 10^3 \Omega \text{ cm}^2$, $1.8 \times 10^3 \Omega \text{ cm}^2$, $4.3 \times 10^3 \Omega \text{ cm}^2$, and $2.5 \times 10^3 \Omega \text{ cm}^2$, respectively. Apparently, the S3 coating showed the best corrosion resistance among the three PEO coatings.

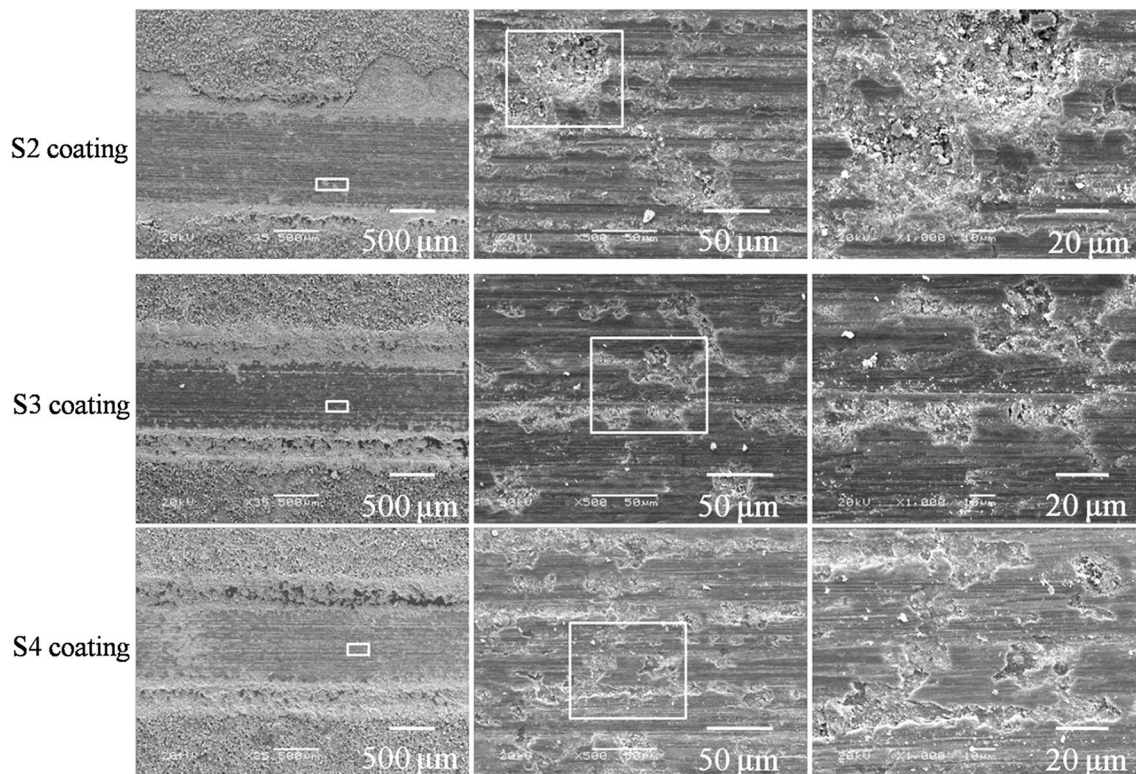


Fig. 8 Morphologies of worn tracks on S2, S3, and S4 coatings

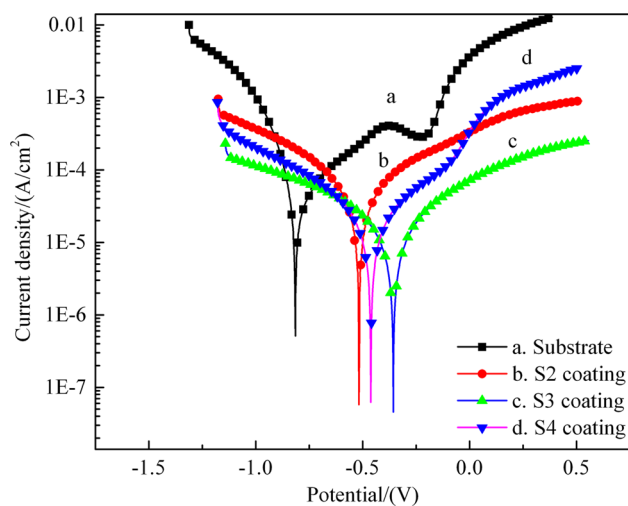


Fig. 9 Potentiodynamic polarization curves of low carbon steel substrate and PEO coatings prepared from electrolytes with different silicate concentrations in 3.5 wt.% NaCl solution

Both the potentiodynamic polarization curves (Fig. 9) and Bode plots (Fig. 10) suggested that the corrosion resistance of the S3 coating was superior to that of the S2 and S4 coatings. The difference in corrosion resistance among the three PEO coatings was attributed to their structure, influenced by the silicate concentration in electrolyte. For the S3 coating, few micropores and microcracks can be found inside the coating or at the interface between coating and substrate. It is difficult for corrosive medium from 3.5 wt.% NaCl solution to penetrate the dense coating to substrate. Therefore, S3 coating showed the best corrosion resistance. In the case of S4 and S2 coatings,

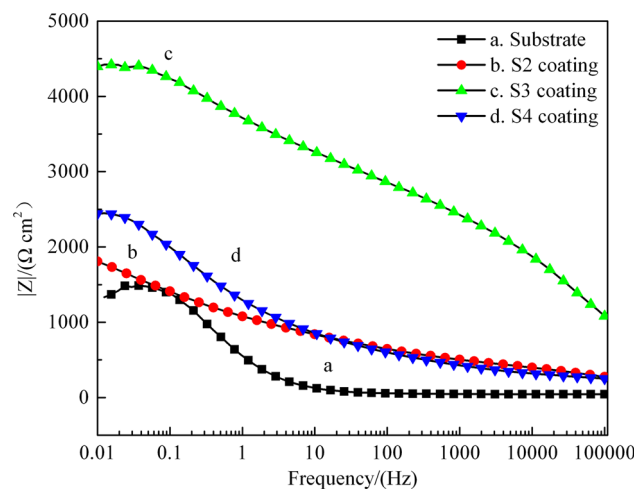


Fig. 10 Bode plots of substrate and PEO coatings prepared from electrolytes with different silicate concentrations in 3.5 wt.% NaCl solution

many micropores and microcracks can be found inside the coating or at the interface between coating and substrate (Fig. 5a and c). The corrosive medium from 3.5 wt.% NaCl solution can easily penetrate the coating through micropores or microcracks to carbon steel substrate, resulting in an inferior corrosion resistance than that of S3 coating.

The morphologies of different PEO coatings after immersion test for 120 h were used to investigate the corrosion behavior and are shown in Fig. 11. In the case of S2 coating and S3 coating shown in Fig. 11(a) and (c), the appearance changed greatly after the immersion test for 120 h. The corrosion products flowed out and nearly sealed the micropores

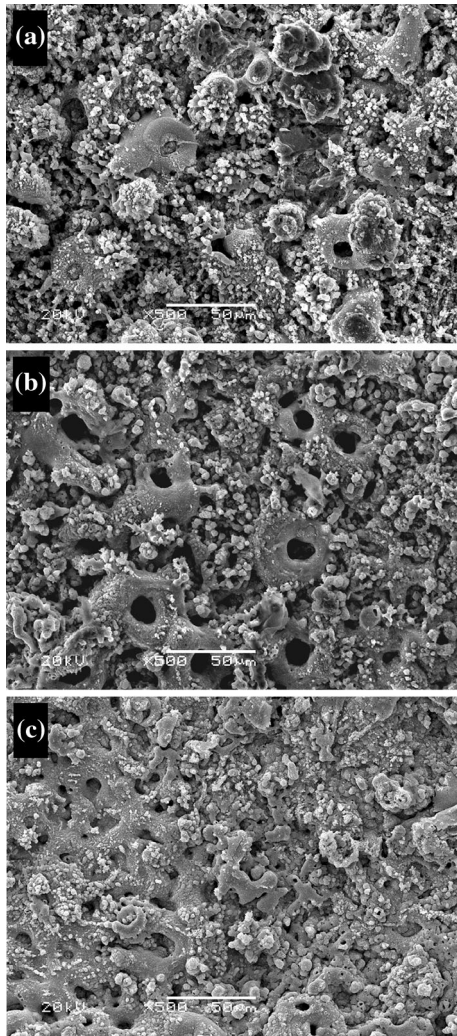


Fig. 11 Morphologies of different PEO coatings after the immersion test for 120 h: a. S2 coating; b. S3 coating; and c. S4 coating

on the surface of S2 and S4 coatings, while for S3 coating depicted in Fig. 11(b), no obvious changes can be observed on the surface. In general, the corrosion resistance of PEO coatings correlated with the structure and the elemental compositions. There is not essential difference among the elemental compositions of S2, S3, and S4 coatings. Therefore, the structure plays a dominant role in determining the anticorrosion property. Comprehensibly, as is shown in Fig. 5(a) and (c), many micropores and microcracks distribute within S2 and S4 coatings. The corrosive medium can easily penetrate the coating to substrate and corrosion products are generated quickly. In the case of S3 coating (Fig. 5b), the structure is denser and few defects can be observed. S3 coating can prevent the corrosive medium from getting to the substrate more effectively.

4. Conclusion

PEO coatings were prepared on low carbon steel from electrolytes with silicate concentrations of 20, 30, and 40 g/L, respectively. Silicate concentration in electrolyte showed no apparent influence on phase composition of PEO coatings.

However, low carbon steel substrate was more prone to be oxidized during the PEO process performed in electrolyte with silicate concentration of 30 g/L, leading to the highest content of Fe and the lowest content of Si in the coating. Moreover, the PEO coating prepared from electrolyte with silicate concentration of 30 g/L was characterized by the densest structure and the best adhesion with substrate. The dense structure and good adhesion of PEO coating are helpful to enhance the wear and corrosion resistance.

References

1. J.D. Liang, S.M. Guo, and Muhammad A. Wahab, Localized Surface Modification on 1018 Low-Carbon Steel by Electrolytic Plasma Process and Its Impact on Corrosion Behavior, *J. Mater. Eng. Perform.*, 1018, **2014**(23), p 4187–4192
2. J.J. Chen, J.L. Li, D.S. Xiong, Y. He, Y.J. Ji, and Y.K. Qin, Preparation and Tribological Behavior of Ni-Graphene Composite Coating Under Room Temperature, *Appl. Surf. Sci.*, 2016, **361**, p 49–56
3. L.M. Berger, Application of Hard Metals as Thermal Spray Coatings, *Int. J. Refract. Met. Hard Mater.*, 2015, **49**, p 350–364
4. E. Machnikova, M. Pazderova, M. Bazzouai, and N. Hackerman, Corrosion Study of PVD Coatings and Conductive Polymer Deposited on Mild Steel, *Surf. Coat. Technol.*, 2008, **202**, p 1543–1550
5. Q.P. Wei, Z.M. Yu, Michael N.R. Ashfold, Z. Chen, L. Wang, and L. Ma, Effects of Thickness and Cycle Parameters on Fretting Wear Behavior of CVD Diamond Coatings on Steel Substrates, *Surf. Coat. Technol.*, 2010, **205**, p 158–167
6. Y. Wang, Z.Q. Huang, Q. Yan, C. Liu, P. Liu, Y. Zhang, C.H. Guo, G.R. Jiang, and D.J. Shen, Corrosion Behaviors and Effects of Corrosion Products of Plasma Electrolytic Oxidation Coated AZ31 Magnesium Alloy Under the Salt Spray Corrosion Test, *Appl. Surf. Sci.*, 2016, **378**, p 435–442
7. J.A. Curran and T.W. Clyne, Porosity in Plasma Electrolytic Oxide Coatings, *Acta Mater.*, 2006, **54**, p 1985–1993
8. M. Vakili-Azghandi, A. Fattah-alhosseini, and M.K. Keshavarz, Effects of Al₂O₃ Nano-particles on Corrosion Performance of Plasma Electrolytic Oxidation Coatings Formed on 6061 Aluminum Alloy, *J. Mater. Eng. Perform.*, 2016, **25**, p 5302–5313
9. Y.L. Wang, Z.H. Jiang, Z.P. Yao, and H. Tang, Microstructure and Corrosion Resistance of Ceramic Coating on Carbon Steel Prepared by Plasma Electrolytic Oxidation, *Surf. Coat. Technol.*, 2010, **204**, p 1685–1688
10. Y.L. Cheng, Z.G. Xue, Q. Wang, X.Q. Wu, E. Matykina, P. Skeldon, and G.E. Thompson, New Findings on Properties of Plasma Electrolytic Oxidation Coatings from Study of an Al-Cu-Li Alloy, *Electrochim. Acta*, 2013, **107**, p 358–378
11. Z.Z. Qiu, R. Wang, Y.S. Zhang, Y.F. Qu, and X.H. Wu, Study of Coating Growth Behavior During the Plasma Electrolytic Oxidation of Magnesium Alloy ZK60, *J. Mater. Eng. Perform.*, 2015, **24**, p 1483–1491
12. M. Babaei, C. Dehghanian, and M. Vanaki, Effect of Additive on Electrochemical Corrosion Properties of Plasma Electrolytic Oxidation Coatings Formed on CP Ti Under Different Processing Frequency, *Appl. Surf. Sci.*, 2015, **357**, p 712–720
13. Y.L. Wang and Z.H. Jiang, In Situ Formation of Low Friction Ceramic Coatings on Carbon Steel by Plasma Electrolytic Oxidation in Two Types of Electrolytes, *Appl. Surf. Sci.*, 2009, **255**, p 6240–6243
14. Y.L. Wang, Z.H. Jiang, and Z.P. Yao, Preparation and Properties of Ceramic Coating on Q235 Carbon Steel by Plasma Electrolytic Oxidation, *Curr. Appl. Phys.*, 2009, **9**, p 1067–1071
15. Y.L. Wang, Z.H. Jiang, and Z.P. Yao, Microstructure, Bonding Strength and Thermal Shock Resistance of Ceramic Coatings on Steels Prepared by Plasma Electrolytic Oxidation, *Appl. Surf. Sci.*, 2009, **256**, p 650–656
16. L.B. Boinovich, S.V. Gnedenkov, D.A. Alpysbaeva, V.S. Egorin, A.M. Emelyanenko, S.L. Sinebryukhov, and A.K. Zaretskaya, Corrosion Resistance of Composite Coatings on Low-Carbon Steel Containing Hydrophobic and Superhydrophobic Layers in Combination with Oxide Sublayers, *Corros. Sci.*, 2012, **55**, p 238–245

17. W.B. Yang, Q.B. Li, Q. Xiao, and J. Liang, Improvement of Corrosion Protective Performance of Organic Coating on Low Carbon Steel by PEO Pretreatment, *Prog. Org. Coat.*, 2015, **89**, p 260–266
18. Mohammad M.S. Al and K.J. Bosta, Ma, Suggested Mechanism for the MAO Ceramic Coating on Aluminium Substrates Using Bipolar Current Mode in the Alkaline Silicate Electrolytes, *Appl. Surf. Sci.*, 2014, **308**, p 121–138
19. L.M. Chang, Growth Regularity of Ceramic Coating on Magnesium Alloy by Plasma Electrolytic Oxidation, *J. Alloys Compd.*, 2009, **468**, p 462–465
20. J.M. Albella, I. Montero, and J.M. Martinez-Duart, A Theory of Avalanche Breakdown During Anodic Oxidation, *Electrochim. Acta*, 1987, **32**, p 255–258
21. A. Ghasemi, N. Schamagl, C. Blawert, W. Dietzel, and K.U. Kainer, Influence of Electrolyte Constituents on Corrosion Behavior of PEO Coatings on Magnesium Alloys, *Surf. Eng.*, 2010, **26**, p 321–327
22. H. Nasiri Vatan, R. Ebrahimi-kahrizsangi, and M. Kasiri-asgarani, Structural, Tribological and Electrochemical Behavior of SiC Nanocomposite Oxide Coatings Fabricated by Plasma Electrolytic Oxidation (PEO) on AZ31 Magnesium Alloy, *J. Alloys Compd.*, 2016, **683**, p 241–255
23. R.O. Hussein, X. Nie, and D.O. Northwood, Influence of Process Parameters on Electrolytic Plasma Discharging Behaviour and Aluminum Oxide Coating Microstructure, *Surf. Coat. Technol.*, 2010, **205**, p 1659–1667
24. X.F. Xu, H.Y. Zhang, Y.M. Chen, N. Li, Y.Y. Li, and L.Y. Liu, SiO₂@SnO₂/Graphene Composite with a Coating and Hierarchical Structure as High Performance Anode Material for Lithium Ion Battery, *J. Alloys Compd.*, 2016, **677**, p 237–244
25. X.P. Lu, M. Mohedano, C. Blawert, E. Matykina, R. Arrabal, K.U. Kainer, and M.L. Zheludkevich, Plasma Electrolytic Oxidation Coatings with Particle Additions—A Review, *Surf. Coat. Technol.*, 2016, **307**, p 1165–1182
26. Q.B. Li, C.C. Liu, W.B. Yang, and J. Liang, Growth Mechanism and Adhesion of PEO Coatings on 2024Al Alloy, *Surf. Eng.*, 2016, <http://doi.org/10.1080/02670844.2016.1200860>
27. F.F. Wei, W. Zhang, T. Zhang, and F.H. Wang, Effect of Variations of Al Content on Microstructure and Corrosion Resistance of PEO Coatings on Mg-Al Alloys, *J. Alloys Compd.*, 2017, **690**, p 195–205
28. J.M. Zhao, X. Xie, and C. Zhang, Effect of the Graphene Oxide Additive on the Corrosion Resistance of the Plasma Electrolytic Oxidation Coating of the AZ31 Magnesium Alloy, *Corros. Sci.*, 2017, **1**, p 5. <https://doi.org/10.1016/j.corsci.2016.11.007>
29. A. Venugopal, J. Srinath, L. Rama Krishna, P. Ramesh Narayanan, S.C. Sharma, and P.V. Venkitakrishnan, Corrosion and Nano Mechanical Behaviors of Plasma Electrolytic Oxidation Coated AA7020-T6 Aluminum Alloy, *Mater. Sci. Eng. A*, 2016, **660**, p 39–46